

On the Detectability of the SZ Effect of Massive Young Galaxies

Daniel Rosa-González^{1,2}, Roberto Terlevich^{1,3}, Elena Terlevich¹★, Amancio Friaça⁴ and Enrique Gaztañaga⁵.

¹ INAOE, Luis Enrique Erro 1. Tonantzintla, Puebla 72840. México.

² Astrophysics Group, Blackett Laboratory, Imperial College, Prince Consort Road, London SW7 2BW.

³ Institute of Astronomy, Madingley Road, CB3 0HA Cambridge, U.K.

⁴ Instituto Astronômico e Geofísico, USP, R. do Matao 1226, Cidade Universitaria, 05508-900, São Paulo, SP, Brazil.

⁵ Institut d'Estudis Espacials de Catalunya. Edifici Nexus, Gran Capita, 2-4, desp. 201, 08034 Barcelona, Spain

Accepted . Received ; in original form 4 November 2018 (ElGaSZ-v105)

ABSTRACT

The Sunyaev-Zel'dovich (SZ) effect expected to be associated with massive star-formation activity produced during the formation of the most luminous bulges of normal galaxies is discussed.

Using 1-D chemohydrodynamical models for spheroidal galaxy evolution we show that during the early epochs of galaxy evolution the gas in massive events of star formation may reach temperatures and densities high enough to produce values of the comptonisation parameter y comparable to those present in galaxy clusters.

In this scenario, we discuss the possibility of detection of the SZ signature in high redshift starforming galaxies with the next generation of mm telescopes capable of arcsecond resolution and equipped with high sensitivity detectors.

We show how millimeter colour–colour diagrams or diagnostic diagrams could be used to distinguish between the dust emission and the SZ effect and suggest the use of simultaneous multifrequency observations to improve the chances of detecting the SZ effect.

Key words: Cosmology: Cosmic Microwave Background, Galaxies: Evolution, Radio: millimetre

1 INTRODUCTION

The SZ effect (Sunyaev & Zel'dovich 1972) is produced when the cosmic microwave background (CMB) photons from the Rayleigh-Jeans region, due to the interaction with the fast electrons, move to the Wien tail of the CMB spectrum thus producing a unique spectral signature. This signature shows an increase with respect to the mean CMB brightness of the observed intensity for wavelengths shorter than 1.34 mm and a decrease for wavelengths longer than 1.34 mm. This is known as the thermal SZ effect. Another component is the kinetic SZ effect, due to the interaction with CMB photons of plasma coherently moving with respect to the reference frame where the CMB is isotropic (e.g. Rephaeli 1995, Birkinshaw 1999, Church, Jaffe and Knox 2001).

The SZ effect constitutes a powerful tool to study the physical properties of the intercluster gas, and when com-

bined with X-ray observations, also to estimate cosmological constants such as the Hubble constant H_0 , the current mass density of the universe Ω_M or the cosmological constant Λ (e.g. Majumdar 2001, Diego et al. 2002, Levine, Schulz & White 2002, Reese et al. 2002, Majumdar & Mohr 2003).

It is understood that in clusters the thermal SZ effect due to the interaction of CMB photons with electrons with temperatures around 10^8 K dominates over the kinetic SZ effect. This fact is evidenced by combining observations at 1 mm where the thermal effect is close to the maximum, at 1.4 mm where it is almost zero and the kinetic SZ effect can be marginally detected and at 2 mm where the thermal SZ has its minimum and is negative (e.g. Lamarre et al. 1998, Mauskopf et al. 2000).

The advent of a new generation of mm telescopes (LMT/GTM or ALMA, described in section 3) that combine relatively high angular resolution with high sensitivity will allow to explore the possibility of detecting the SZ effect in volumes much smaller than that of a cluster of galaxies.

★ Visiting Fellow at IoA, UK

Would it be possible for these new instruments to detect the SZ signature in individual galaxies?

Natarajan & Sigurdsson (1999), Rosa-González et al. (2000, 2001), Majumdar, Nath and Chiba (2001) and Rosa-González (2002) have indeed explored the detectability of the SZ effect in individual galaxies.

Natarajan & Sigurdsson (1999) studied the SZ effect due to galactic outflows powered by the mechanical energy provided by the accretion of matter to the central supermassive black hole in QSOs. Majumdar et al. (2001) propose the evolution of supernova driven galactic winds during the early stages of evolution of a normal galaxy, as the cause of the distortion of the CMB radiation due to the kinetic SZ effect. A similar model was originally proposed by Tegmark, Silk and Evrard (1993) to explain the absence of absorption lines in the observed spectra of high redshift quasars (Gunn-Peterson effect, Gunn & Peterson 1965). The explosion model assumes an initial energy input which is equal to the 2% of the total luminosity generated in the supernova explosions during about 5×10^7 years. The range of galaxy masses covered by this model goes from $5 \times 10^7 M_\odot$ to $10^{11} M_\odot$.

Rosa-González et al. (2000, 2001) and Rosa-González (2002) discussed the possibility of observing the SZ effect in the centre of young giant spheroidal galaxies. They include in the calculations both the thermal and the kinetic SZ effect.

In the *accepted* galaxy formation scenario described by the hierarchical model (e.g. Navarro, Frenk & White 1995), massive galaxies form after merging with smaller system that have been formed in a previous epoch. However, there is observational evidence that a significant number of L^* galaxies exist at redshift of about 5 and beyond (Hu, Cowie & McMahon 1998, Stanway, Bunker & McMahon 2003). Jimenez et al. (1999) discussed the possibility of the existence of massive elliptical galaxies at high redshift, contrary to early predictions of the hierarchical models of galaxy formation. The study of massive galaxies at high redshift that could be detected through the unique SZ signature could be used to constrain the different galaxy formation scenarios.

The SZ effect due to young galaxies together with radio sources (Holder 2002) and dusty galaxies (Blain, Ivison & Smail 1998, Blain 1998) are potential sources of noise in sensitive studies of SZ clusters and upcoming measurements of the CMB fluctuations (e.g. *FIRST*, *Plank*). Therefore, their characteristic emission and physical scale must be quantified.

In this paper we explore in detail the possibility of detection of the SZ effect in young galaxies undergoing a massive starformation event. We discuss the confusion due to dust emission and suggest a diagnostic to segregate between dust emission and SZ effect distortions.

1.1 Thermal SZ effect

The SZ effect describes the brightness change of the CMB due to the inverse Compton scattering by hot electrons (Sunyaev & Zel'dovich 1972).

The change in intensity between the unaffected CMB radiation and the radiation which go through the hot gas can be expressed by the integral,

$$\Delta I = \tau_e \frac{2h}{c^2} \int_{-\infty}^{+\infty} ds P(s) \left[\frac{\nu_0^3}{\exp\left(\frac{h\nu_0}{kT_{rad}}\right)} - \frac{\nu^3}{\exp\left(\frac{h\nu}{kT_{rad}}\right)} \right] \quad (1)$$

where the energy of the CMB photons is given by $h\nu_0$, the energy of the photons which come out from the cluster is $h\nu$, s is defined by $s = \log(\nu/\nu_0)$, τ_e is the optical depth for scattering and $P(s)$ is the probability that an incident photon with energy $h\nu_0$ becomes a photon with an energy $h\nu$ (Birkinshaw 1999).

The integral in the Equation 1 can be calculated by using the non relativistic expression given by the Kompaneets approximation (Kompaneets 1957),

$$\Delta I(x) = h(x)yI_0 \quad (2)$$

where the distortion of the photon spectrum, $h(x)$ is defined by

$$h(x) = x^4 \frac{e^x}{(e^x - 1)^2} \left(x \coth \frac{x}{2} - 4 \right) \quad (3)$$

x is the dimensionless frequency, $x = h\nu/(kT_{rad})$ with $T_{rad} = 2.728$ the temperature of the CMB,

$$I_0 = \frac{2h}{c^2} \left(\frac{k_B T_{rad}}{h} \right)^3 \quad (4)$$

and the Comptonization parameter “ y ” is defined by the integral of the electron pressure along the line of sight

$$y = \sigma_T \int dl n_e \frac{k_B T_e}{m_e c^2} \quad (5)$$

In this equation σ_T is the Thomson scattering cross section, n_e and T_e are the electron number density and the electron temperature respectively, k_B is the Boltzmann constant and $m_e c^2$ is the rest energy of an electron; (see Rybicki & Lightman 1980 for a more detailed derivation of the different expressions described above and Birkinshaw 1999 for a recent review). The effect of the hot gas on the CMB spectrum is to produce a fractional change in the brightness of the CMB radiation. We remark that the amplitude of the SZ effect is redshift-independent and depends only on the integrated properties of all the hot gas along the line of sight. The SZ effect can be considered as a tool to detect high pressure electron gas over cosmological distances.

1.2 Kinetic SZ effect

The kinetic SZ effect, as already mentioned, is due to the movement of the plasma with respect to the CMB rest frame. For a shell of matter which is moving with a radial velocity v with respect to the Hubble flow, the change of the intensity due to the kinetic SZ effect (ΔI_{kin}) is given by,

$$\Delta I_{kin} = -\frac{v}{c} \tau_e I_0 \frac{x^4 e^x}{(e^x - 1)^2} \quad (6)$$

where τ_e is the scattering optical depth, I_0 is given by equation 4 and x is the dimensionless frequency.

At low frequencies, the ratio between the kinetic SZ effect (ΔI_{kin}) to the thermal SZ effect (ΔI_{th}) is independent of the scattering optical depth and can be calculated by,

$$\frac{\Delta I_{kin}}{\Delta I_{th}} = \frac{1}{2} \frac{v m_e c^2}{c k T_e} \quad (7)$$

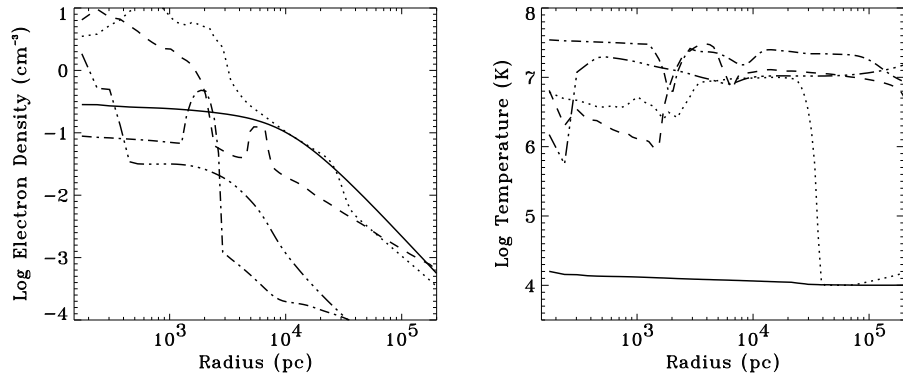


Figure 2. Electron density and temperature profiles for the model of baryonic mass $2 \times 10^{12} M_{\odot}$. The different lines correspond to different times: 20 Myr for the solid line, 600 Myr for the dotted line, 1 Gyr for the dashed line, 4 Gyr for the dot-dashed line and 11 Gyr for the dot-dot-dashed line.

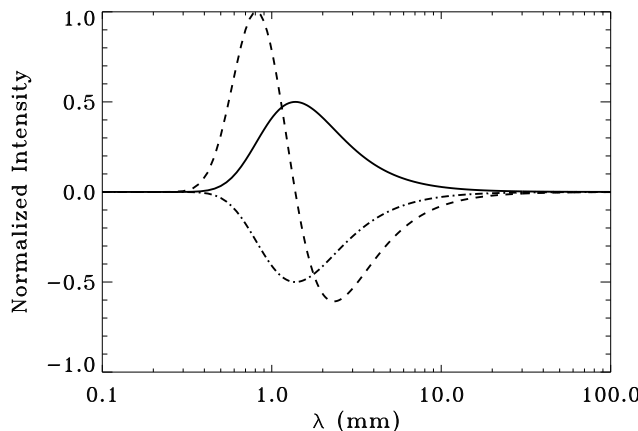


Figure 1. The kinetic SZ effect (solid and dot-dashed lines) signature is compared to the thermal SZ effect (dashed line) for the case where the kinetic effect is half of the thermal one. The two cases of the kinetic SZ effect correspond to gas moving away from (dot-dashed line) and towards (solid line) the observer.

where v is the velocity of the flow, $m_e c^2$ is the electron rest energy and T_e is the gas temperature (Birkinshaw 1999). The signatures of the thermal and kinetic SZ effects are plotted in Figure 1.

2 THE GALAXY FORMATION MODEL

In order to estimate the amplitude and time evolution of the SZ effect for individual galaxies, it is necessary to know the time and radial dependence of the gas temperature, density and velocity. We have restricted our study to those stages of galaxy evolution characterized by a high injection rate of mass and energy into the galaxy ISM (which happens to occur during the first few Gyr of the galaxy evolution). We have further assumed that this occurs during a maximum in the star formation rate produced by any of the known mechanisms.

The evolution and radial profiles mentioned above (Fig-

ure 2) have been obtained from a chemohydrodynamical model for evolution of elliptical galaxies (Friaça & Terlevich 1998, hereafter FT98). The model combines multi-zone chemical evolution with 1-D hydrodynamics to calculate the evolution of chemical abundances in gas and stars, and also the temperature, density and velocity profiles of the gas. In this way, we can calculate the y profiles which are used to estimate the flux collected by a given beam size at a given frequency.

In the FT98 model, a single massive dark halo hosts baryonic gas that falls toward the centre of the dark halo and will subsequently form stars. The dark halo is given by a static mass density distribution $\rho_h(r) = \rho_{h0}[1 + (r/r_h)^2]^{-1}$, where ρ_{h0} is the halo central density and r_h is the halo core radius. The gas and the stars exchange mass through star formation and stellar mass losses (supernovae, planetary nebulae, and stellar winds). Both the stellar distribution and the dark halo are truncated at a common tidal radius r_t . The system, assumed to be spherical, is subdivided in several spherical zones and the hydrodynamical evolution of its ISM is calculated. The equations of chemical evolution for each zone are then solved taking into account the gas flow, and the evolution of the chemical abundances is obtained. A total of ≈ 100 star generations are stored during 13 Gyr for chemical evolution calculations. We assume that at a given radius r and time t , the specific star formation rate $\tilde{\nu}(r, t)$ follows a power-law function of gas density (ρ): $\tilde{\nu}(r, t) = \nu(\rho/\rho_0)^{1/2}$, where ρ_0 is the initial average gas density inside r_h , and ν is the normalization of the star formation law. We include inhibition of star formation for expanding gas ($\nabla \cdot u > 0$) or when the density is too low, and, therefore, the cooling is inefficient (i.e., for a cooling time $t_{coo} = (3/2)k_B T / \mu m_H \Lambda(T) \rho$ longer than the dynamical time $t_{dyn} = (3\pi/16 G \rho)^{1/2}$) by multiplying $\tilde{\nu}$ as defined above by the inhibition factors $(1 + t_{dyn} \max(0, \nabla \cdot u))^{-1}$ and $(1 + t_{coo}/t_{dyn})^{-1}$. A characteristic of these models is that several episodes of inflow and outflow occur simultaneously at different radii. The chemodynamical model for spheroids was used to investigate the relation between young elliptical galaxies and QSO activity (FT98), the absence of passively evolving elliptical galaxies in deep surveys (Jimenez et al.

1999), Lyman Break Galaxies (Friaça & Terlevich 1999), Blue Core Spheroids (Friaça & Terlevich 2001), the coupled spheroid and black hole formation (Archibald et al. 2002), and the link between DLAs and dwarf galaxies (Lanfranchi & Friaça 2003).

The models are parameterized according to the (initial) baryonic mass inside the tidal radius, $M_G = M_g + M_*$, r_h , r_t , and the ratio of the halo to the (initial) luminous mass, M_h/M_G . We have investigated a grid of runs with M_G between 10^{11} and $5 \times 10^{12} M_\odot$, and r_h in the range 2.5–15 kpc (see FT98). We set $r_t = 28r_h$ and $M_h/M_G = 5$. That value is compatible with the recent WMAP results where the baryon density $\Omega_b = 0.047 \pm 0.006$ and the matter density $\Omega_M = 0.29 \pm 0.07$ (Spergel et al. 2003). Smaller (larger) values of the ratio dark matter versus baryonic mass do not significantly alter the observed fluxes, but due to the shallower (deeper) potential well, the galactic winds will appear earlier (later). For example, in the model with $M_G = 10^{12} M_\odot$, the galactic wind occurs at 1.51, 1.55 and 1.67 Gyr, for $M_h/M_G = 3, 5$ and 7.5 respectively.

The chemical evolution is driven by the stellar winds, planetary nebulae and SN phase which produce the enrichment of the ISM. New generation of stars form in the more metal-rich medium. We do not assume instantaneous recycling approximation for the chemical enrichment, but instead we take into account the delays for gas restoring from the stars due to the main-sequence lifetimes. Instantaneous mixing with the ISM is assumed for the stellar ejecta. We use metallicity dependent yields for SNe II, SNe Ia, and intermediate mass stars (IMS): the SNe II yields of Woosley & Weaver (1995), for metallicities $Z/Z_\odot = 0, 10^{-4}, 10^{-2}, 10^{-1}$ and 1; SNIa yields from Iwamoto et al. (1999) — their models W7 and W70 (progenitor metallicity $Z=Z_\odot$ and $Z=0$, respectively); the yields for IMS ($0.8 - 8 M_\odot$), with initial $Z=0.001, 0.004, 0.008, 0.02$ and 0.4 , from van den Hoek & Groenewegen (1997) (their variable η_{AGB} case). For more details of the nucleosynthesis prescriptions, see FT98. The models start with an entirely gaseous protogalaxy with primordial chemical abundances ($Y = 0.24$, $Z = 0$).

In the FT98 models there is self-consistency of the hydrodynamics, chemical evolution and atomic physics, since the cooling function is evaluated based on the actual chemical abundances obtained from the chemo-dynamical modelling. For the sake of simplicity, our cooling function is a function only of the abundances of O and Fe, which are the main coolants for $T > 10^5$ K. In the calculation of the cooling function, the abundances of elements other than Fe and O have been scaled to the O abundance as $n_i = n_{i,P} + (n_{i,\odot} - n_{i,P})n_O/n_{O,\odot}$, where n_i is the ISM abundance by number of the element i , $n_{i,P}$ its primordial abundance and $n_{i,\odot}$ its solar abundance [the photospheric values of Holweger (2001) for N and O, and the meteoritic values of Grevesse & Sauval (1998) for the other elements].

It is important to note that the FT98 models describe the evolution of isolated galaxies and do not take into account effects such as mergers that play an important role in structure formation within hierarchical galaxy formation models. However, the FT98 models can be considered as a description of the evolution of the hot gas after a major star forming event produced by interaction or merger. In addition, while the present chemodynamical model accounts for complex flow patterns, with inflow in some regions and out-

flow in other regions, the model does not take into account asymmetric fluxes due to the assumed spherical symmetry. Despite the limitations due to the spherical symmetry, the detailed predictions of this model are useful due to the good radial resolution of the galaxy and the realistic treatment of the star formation and proper calculation of the chemical evolution of the gas and stars. The FT98 model represents a complementary tool to the semi-analytic models of galaxy formation, which currently adopt very simplified recipes of star-formation but with coarser space resolution (e.g. Somerville & Primack 1999, Benson et al. 2001).

An important aspect relevant to the present calculation is that the models provide an estimate of the size of the hot gas region. This is central for deriving the expected flux because the effective y parameter (which is the average of the y parameters within a given beam size, Section 2.1) depends strongly on the size of the telescope beam.

2.1 The SZ effect in massive young galaxies.

The FT98 models predict that the hot gas in massive star forming regions with ages between 10^8 and 10^9 years can reach temperatures exceeding 10^7 K and densities higher than 1 cm^{-3} within a radius of a few kpc. These temperatures and densities imply values of the Comptonization parameter y larger than 10^{-4} . The maximum temperatures of the gas in the models (~ 1 keV) are well below the relativistic limit (~ 500 keV), and, therefore, we use the non-relativistic approximation (e.g. Birkinshaw 1999) to estimate the SZ effect (Equation 2). Notice that the central y parameter is calculated for a region of a few hundred parsecs across. Only in this region is the y parameter comparable to those observed in galaxy clusters.

Figure 3 shows the variation of the thermal parameter (y_{th}) with radius. In the beginning of the calculations (the $t = 20$ Myr lines in Figures 2 and 3), the gas has not yet settled in the potential well of the galaxy and its density is low and temperature is cold everywhere (the model initial conditions assume gas at $T = 10^4$ K), and, as a consequence, y is very small. As the model evolves, the gas falls towards the centre and is compressed, giving rise to shocks that rapidly heat the gas in the core to approximately the virial temperature of the system ($T \sim 10^7$ K). Then, a highly efficient star formation is occurring throughout the galaxy and a young stellar population is rapidly built up. Following the initial violent star formation burst, the first Type II SNe appear and heat the ISM. The star formation is vigorous and intense during the first ~ 0.5 Gyr, when nearly half of the stellar population is formed. In Figures 2 and 3, we see that at $t = 0.6$ Gyr, there is enough gas at temperatures around $T = 10^7$ K to maintain values of y close to 10^{-4} in the central kpc. At 1 Gyr since the start of the calculations, the star formation gas consumed most of the gas and the SNI (and SNIa) heating is past its maximum. Although the gas temperature is higher than before, its density has dropped along most of the galaxy, resulting in a significant decrease of y . As the galaxy evolves, the star formation rate decreases, the main heating source of the ISM is provided by Type Ia supernovae. Eventually, the thermal energy of the gas is enough to overcome the escape velocity, and the remaining gas is expelled from the galaxy by galactic winds. At this point, the primary burst of star formation ceases.

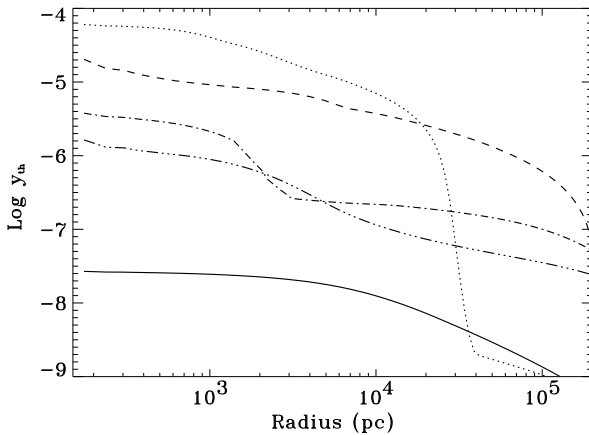


Figure 3. The thermal y parameter as a function of radius. Different lines correspond to different times: 20 Myr for the solid line, 600 Myr for the dotted line, 1 Gyr for the dashed line, 4 Gyr for the dot-dashed line and 11 Gyr for the dot-dot-dashed line. The baryonic mass of the galaxy is $2 \times 10^{12} M_{\odot}$.

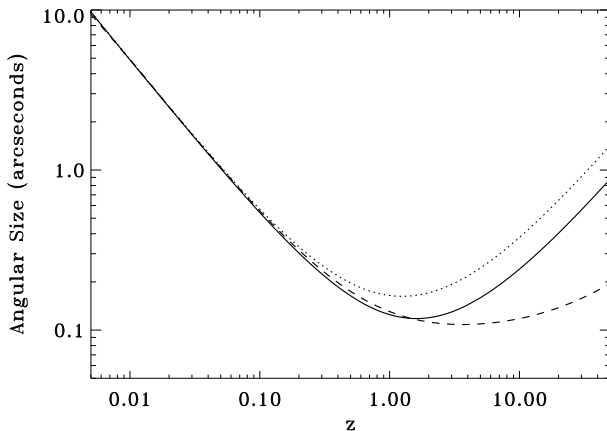


Figure 4. Angular size corresponding to a physical size of 1 kpc for different cosmologies. The solid line is the result for a universe with $\Omega_M = 0.3$ and $\Omega_\Lambda = 0.7$. The dotted line is for the case of $\Omega_M = 1$ and $\Omega_\Lambda = 0$ and the dashed line is for $\Omega_M = 0.05$ and $\Omega_\Lambda = 0$.

The curves at $t = 4$ and 11 Gyr illustrate the post-galactic wind stage, when the gas temperature is high, but the low density implies a low y .

The y parameter is smaller in the external layers where the pressure is lower, therefore the resulting y parameter averaged within the telescope beam is expected to be lower than the central one. This effect can be quantified by an effective y parameter (y_{eff}) defined as the average of the y parameter in the different shells weighted by the corresponding projected area and convolved with the telescope beam profile,

$$y_{eff} = \left(\frac{1}{\theta^2} \int y d\theta \right) * B(\theta) \quad (8)$$

where θ is the size of the telescope beam and $B(\theta)$ is the telescope beam profile.

In reality, the telescope beam will cover a variable frac-

tion of the galaxy depending on its intrinsic size, its redshift and the adopted cosmology (Figure 4). In order to translate physical sizes to angular sizes, we adopted a cosmological model given by $\Omega_M = 0.3$, $\Omega_\Lambda = 0.7$ and $h=0.7$.

To illustrate the effect of beam dilution we show in Figure 5 the change of y_{eff} with respect to the beam angle for models at 400 Myr. The results are similar for different times. The behaviour of y_{eff} can be analysed in three separate cases, according to the beam size:

- **Small beam**, y_{eff} increases as θ^2 , where θ is the size of the beam. In this case the beam size is smaller than the first radius of the model at the given time, so the value of y increases until the telescope beam reaches the inner radius of the model galaxy.

- **Medium beam**, for beam angles similar to the inner radius, the model obtains the maximum value of y which corresponds to the central one (y_c). The integrated pressure in the external layer is lower than in the inner ones, hence increasing the beam size produces a slight decrease of y_{eff} .

- **Large beam**, when the size of the beam is larger than the region where the values of y are significant the averaged y goes down as θ^{-2} . Notice that for the most massive galaxy (baryonic mass $5 \times 10^{12} M_{\odot}$) the fast decline is reached after an angle of about $10''$ but for the low mass galaxies the fast decline starts when the angle is about $1''$.

Figure 6 shows that for the massive galaxies, the comptonisation parameter reaches values higher than 3×10^{-5} . In the case of quasar outflows, Natarajan & Sigurdsson (1999) estimated a value for the comptonisation parameter of about 5×10^{-5} . Similar values of the comptonisation parameter were estimated for the case of early galactic winds (Majumdar et al. 2001).

However, the dilution effect produces a significant decrease of the y parameter and consequently a smaller expected flux (Figure 6). Using the output of the models, we obtained the effective y parameter as a function of time and beam angle. The behaviour of the central y and the effective y parameter for the case of a beam of $5''$ is plotted in Figure 6. The central y parameters have the maxima between 150×10^6 years and 10^9 years, independently of the baryonic mass of the galaxy. The maximum values go from 2×10^{-4} for galaxies with baryonic masses of 5×10^{12} and $2 \times 10^{12} M_{\odot}$ down to 3×10^{-5} for galaxies with baryonic masses of $10^{11} M_{\odot}$. The effective y within an angle of $5''$ is about 10 times lower than the central one (Figure 6). The given times in Figures 6, 7 and 9 correspond to galaxies which started to collapse at redshift 50. Within this initial conditions, the maximum SZ amplitude is reached at redshifts between 12 and 5.

2.2 The kinetic SZ effect in young galaxies

There are two processes that could produce a significant kinetic SZ effect in young galaxies. One is the infall of the primordial gas to the center of the galaxy and the other is the outflow produced by SN explosions and winds from massive young stars.

The calculations of the thermal SZ effect presented in the previous section, are for a spherical galaxy (the models by FT98 on which the calculations are based, assume spherical symmetry). For the case of the kinetic SZ effect

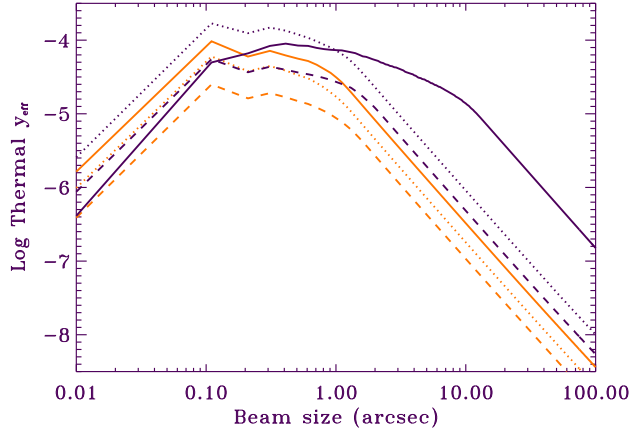


Figure 5. The lines represent the variation of the beam averaged y parameter with beam size for a fixed time of 4×10^8 years, corresponding to galaxies of baryonic masses of $10^{11} M_{\odot}$ (grey dashed line), $2 \times 10^{11} M_{\odot}$ (grey dotted line), $5 \times 10^{11} M_{\odot}$ (grey solid line), $10^{12} M_{\odot}$ (black dashed line), $2 \times 10^{12} M_{\odot}$ (black dotted line) and $5 \times 10^{12} M_{\odot}$ (black solid line).

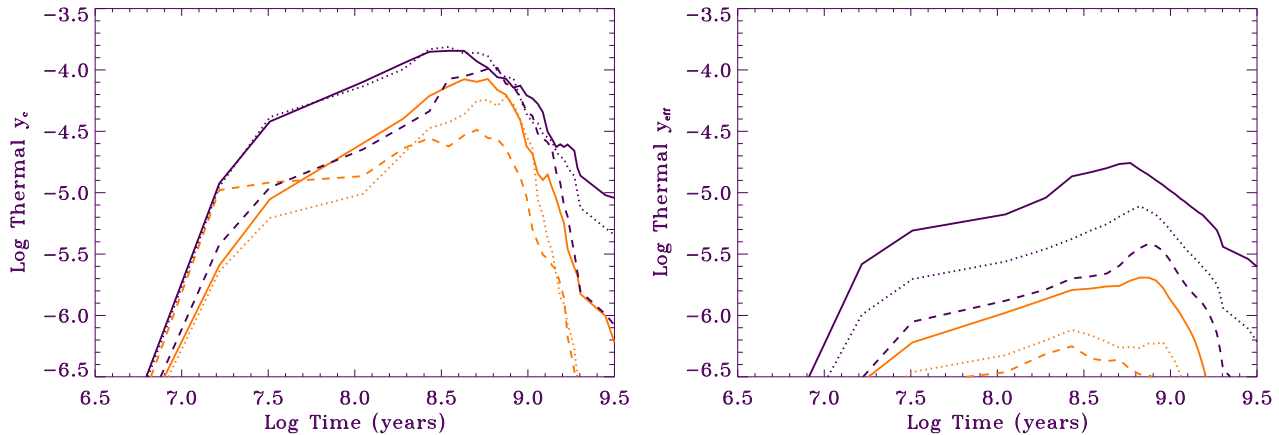


Figure 6. Evolution of the y parameter. The left panel is the evolution of the central thermal y parameter (y_c). The right panel is the effective thermal y parameter (y_{eff}) assuming a beam size of $5''$. The different lines correspond to different galaxy masses, coded as in Figure 5.

of a spherical galaxy with isotropic winds, the total contribution to the kinetic y parameter becomes zero. In reality, the geometry of galactic winds tend to be more bi-conical than spherical. If there is asymmetry between the two cones, there will be a net kinetic SZ effect. Even within the context of our spherically symmetric calculations, we can estimate the kinetic SZ effect, in the case of extreme asymmetry, by considering the contribution of only one hemisphere of the galaxy.

In this gross approximation, the kinetic effect is dominant at early phases of the galaxy evolution (less than 0.5 Gyr) due to the infall of gas to the centre of the galaxy. During this epoch the gas is relatively cold with temperatures of about 10^4 K favouring the kinetic effect over the thermal one. During this early phase the SZ kinetic effect could be several times higher than the thermal effect (Figure 7). In the central region of the galaxy the thermal effect dominates due to the high temperatures and densities and as a result the central y_{th} parameter is higher than the kinetic component.

Notice, however, that an assumption of extremely asymmetric infall is probably less justified than that of asymmetric wind. However, when the galactic wind is operating ($t > 1$ Gyr) due to its low density, the implied kinetic SZ effect would be much less than the thermal SZ effect. Moreover at these late times, the galaxy is far from the time of maximum SZ effect ($t \sim 0.5$ Gyr).

3 TELESCOPES AND DETECTORS

There are a few future mm and sub-mm facilities that may be capable of detecting the SZ effect produced by individual galaxies.

One is the Atacama Large Millimeter Array (ALMA), a project lead by institutions of Europe, Japan and North America. ALMA will be an array of 64 antennas of 12 m in diameter getting baselines up to 10 km. It is expected that ALMA will cover the wavelength range from 8 mm to $350 \mu\text{m}$ (Blain 1999). It will be situated in the Atacama desert in Chile.

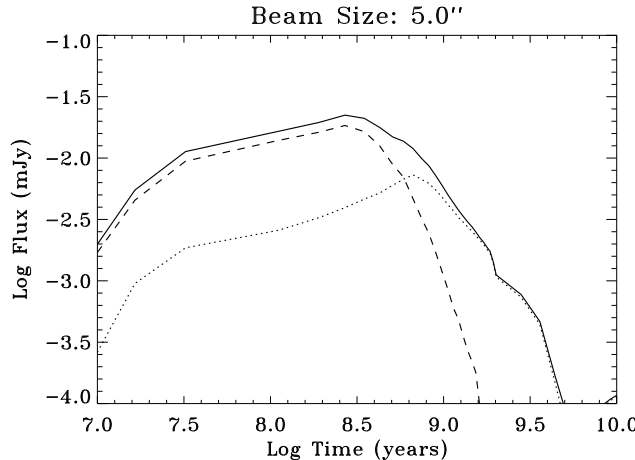


Figure 7. The total flux (solid line) due to the sum of the thermal (dotted line) and kinetic (dashed line) SZ effects for a galaxy of $2 \times 10^{12} M_{\odot}$ (baryonic mass). We assumed that the kinetic effect has a positive sign so the corresponding flux is added directly to the flux due to the thermal SZ. The beam angle ($5''$) corresponds to observations at 1 mm with a 50 meter telescope.

Another one is the Large Millimeter Telescope (LMT/GTM), a binational project between UMASS (USA) and INAOE (México), with a single dish antenna of 50 m diameter. It will be situated on the Cerro la Negra in México. In the case of observations of the continuum, that is the case of the SZ effect, the LMT/GTM will be equipped with BOLOCAM, a sensitive wide field camera that will operate between 3 and 1 mm. At 1 mm on the LMT/GTM, BOLOCAM will have a projected pixel size of $5''$, three times smaller than SCUBA on the JCMT observing at $850 \mu\text{m}$ (Holland et al. 1998).

We have also included the characteristics of the Green Bank Telescope (GBT) a 100 m single dish which is planned to be able to work at 3 mm in the next few years (Dicker 2002).

The mapping speed is defined as the ratio between the field of view (FOV) and the square of the sensitivity. High mapping speed is necessary to complete surveys covering big portions of the sky and to detect the fainter sources.

Table 1 shows the sensitivity, FOV and mapping speed for the different telescopes. The sensitivity of BOLOCAM in the LMT/GTM is estimated from Glenn et al. 1998. The sensitivity and FOV of ALMA are from Blain (1999). Notice that ALMA is not designed to perform wide area surveys (so it does not have an associated mapping speed).

We are interested in the detection of the SZ effect in young massive galaxies that at high redshift may have a few arcseconds in size and an estimated flux of several μJy (See Section 2.1). Table 1 shows that only with the next generation of mm telescopes it may be possible to detect them.

4 THE EFFECT OF DUST EMISSION

Dust emission is a dominant component in the observed multifrequency spectrum of galaxies over a wide range of redshifts. Given the small signal associated with the SZ of individual galaxies, dust emission will probably dominate

the mm spectrum making difficult the detection of the SZ signature. At high redshift the peak of the dust emission ($\sim 100 \mu\text{m}$) moves to sub-mm and mm wavelengths (e.g. Rowan-Robinson et al. 1997, Hughes et al. 1998) i.e. over the region where the SZ effect has its maximum.

We estimated the relative amplitude of the flux due to the SZ effect and that due to the dust by comparing the mm flux due to dust emission in M82, a well known starforming galaxy, with the expected flux due to the SZ effect.

M82 is a nearby (~ 3.2 Mpc) starburst galaxy with an infrared luminosity of $L(8 - 1000 \mu\text{m}) = 3 \times 10^{10} L_{\odot}$ which represents the 84% of the total galaxy luminosity (Telesco 1988). Hughes, Gear and Robson (1994) showed that the spectral distribution of energy in the sub-mm range of M82 is well fitted by a grey body law with a temperature of 48 K and an emissivity index of 1.3.

The dust emission is,

$$F_{\nu} = M_{dust} k_d^{rest} B(\nu^{rest}, T) \frac{1+z}{D_L^2} \quad (9)$$

where z is the redshift of the source, k_d^{rest} is the rest-frequency mass absorption coefficient (e.g. Rowan-Robinson 1986), $B(\nu^{rest}, T)$ is the rest-frequency value of the Planck function for dust at temperature T , D_L is the luminosity distance and (M_{dust}) is the total mass of dust (Hughes, Dunlop and Rawlings 1997). For the rest-frequency mass absorption coefficient (k_d^{rest}) we adopted the value of $0.15 \text{ m}^2 \text{kg}^{-1}$ as suggested by Hughes et al. (1997). The dependence of k_d with wavelength is given by $k_d \propto \lambda^{-\beta}$, where β is the emissivity index of the dust grains.

Observations of galaxies with different sources of heating indicate an average dust grain temperature of about 50 K (e.g. Chini et al. 1989, Chini, Kreysa and Biermann 1989, Hughes et al. 1993, Hughes et al. 1994). In what follows we assume a dust temperature of 50 K and an emissivity index of 1.5 given by Hughes et al. (1997). The dust mass of M82 is about $2 \times 10^6 M_{\odot}$ (Hughes et al. 1994). We also compare the flux due to dust in galaxies hundred times brighter than M82 (Arp 220-like luminosity, Figure 8) to the flux due to the SZ effect (Figure 7). We must keep in mind that Arp 220 is an extreme case of an ultraluminous infrared galaxy (ULIRG) with an infrared luminosity of about $\sim 10^{12} L_{\odot}$ which corresponds to 98% of the total luminosity. Combining the observed flux at $850 \mu\text{m}$ ($F(850 \mu\text{m}) = 792 \pm 26 \text{ mJy}$) given by Lisenfeld, Isaak and Hills (2000) with Equation 9 we estimate for Arp 220 a dust mass of about $10^8 M_{\odot}$. A value of $2 \times 10^8 M_{\odot}$ for the dust mass is given by Dunne et al. (2000) assuming a dust temperature of 42.2 K and an emissivity index of 1.2.

Galaxies as M82 have an expected flux at 1 mm of about $20 \mu\text{Jy}$ for redshifts between 1 and 10 and about $5 \mu\text{Jy}$ for observations at 2 mm (100 times higher for the case of an Arp 220-like galaxy). Notice that these values are similar to the maximum values of the fluxes due to SZ emission for massive galaxies with baryonic masses higher than $10^{11} M_{\odot}$ (Figure 7). The estimate of total fluxes due to dust, does not take into account the relative size of the galaxy since the SZ flux plotted in Figure 7 corresponds only to the flux estimated inside a beam size of $5''$. At high redshift ($z > 3$) the whole galaxy will fill the $5''$ beam, but probably will be resolved by interferometric observations. The other fact is that the dust content of M82 does not change

Table 1. Main characteristics of the most sensitive telescopes at the mm range. The upper value of 10 km for ALMA correspond to the maximum separation between two antennas. The mapping speed (*) is measured in $\frac{\text{arcmin}^2}{\text{hour mJy}^2}$.

Telescope and diameter	Camera	Wavelength (mm)	Angular Resolution (arcsec)	Sensitivity (mJy/ $\sqrt{\text{Hz}}$)	FOV (arcmin 2)	Mapping Speed (*)
JCMT (15 m)	SCUBA	0.85	15	90	2	0.9
GBT (100 m)	3mm-Camera	3.00	8	0.2	0.3	27000
LMT/GTM (50 m)	BOLOCAM	1.2	6	2	2	1800
ALMA (< 10 km)	–	1.30	0.03	0.46	0.16	–

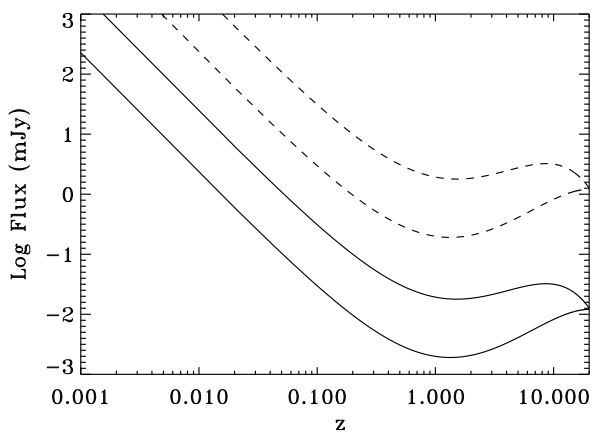


Figure 8. The solid lines are the expected flux for M82 at 2 mm (lower solid line) and at 1 mm (upper solid line) assuming a dust temperature of 50 K and $\beta = 1.5$. The dashed lines are the expected flux for a galaxy 100 times more luminous than M82. The lower dashed line corresponds to fluxes at 2 mm and the upper dashed line, to fluxes at 1 mm.

with time, therefore the fluxes in Figure 8 can be considered upper limits for galaxies with lower metal content or less evolved than M82.

5 DIFFERENTIAL MAPPING AND THE MM COLOUR-COLOUR DIAGRAM

The particular spectral signature of the SZ effect, i.e. a positive maximum at about 800 μm and a negative minimum at around 2 mm plus its non-dependence on redshift can be used to maximize its detection against the dust emission from the same source.

Using the fact that at 2 mm the SZ has a negative value, the difference between the flux at 1 mm and the flux at 2 mm (Figure 9) is almost two times the signal given by the individual values (Figure 7). Notice that subtracting the signal at 1 mm from the signal at 2 mm will also cause a decrease in the flux due to sources dominated by dust emission therefore producing a map biased to SZ sources. Source confusion due to dust emission should also be reduced. This differential mapping method will also help in removing the sky signal as at these low resolutions the atmosphere emission at 1 mm and at 2 mm are correlated. In a single observation with a wide area camera, the sky signal is removed by using the fact that some of the pixels are viewing the

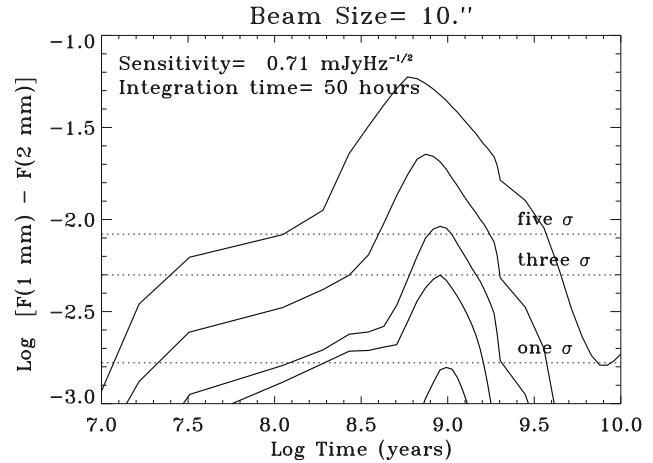


Figure 9. Difference between the fluxes at 1 mm and at 2 mm. The different lines correspond to different galaxy masses; from the bottom to the top the baryonic masses are 2×10^{11} , 5×10^{11} , 10^{12} , 2×10^{12} and $5 \times 10^{12} M_{\odot}$. Only the thermal SZ was included in this figure. The horizontal dotted lines are the estimated rms assuming the sensitivity and integration time shown in the upper left corner.

blank sky. Subtracting the time average level of these blank pixels can increase the signal to noise by a factor of 3. This is possible because the source structure is constant in time while the sky vary over the array on time scales of several seconds (Holland et al. 1998). The use of simultaneous measurements at different wavelengths allows to reduce the sky noise due to a better sampling of the fast sky fluctuations. Also it is possible to separate different components of the image (i.e. detector noise, sky, astrophysical signal) without assuming any atmospheric spectrum by solving a set of coupling equations and obtaining a model of the sky brightness distribution (Mauskopf et al. 2003).

To distinguish between galaxies which are dominated by the dust emission and galaxies which are dominated by the SZ effect, we have explored the use of mm colour-colour diagnostic diagrams.

Let us consider the emission of an object composed by the thermal SZ effect with a fixed comptonization parameter of 10^{-4} plus a grey body. The amplitude of the grey body emission is given by changing \mathbf{R} which is the ratio between the maximum of the grey body emission and the maximum of the SZ emission (Figure 10).

Figure 11 represents the plane $I(2 \text{ mm})/I(1 \text{ mm})$ vs. $I(3 \text{ mm})/I(1 \text{ mm})$ given by the ratios between the intensities at the given wavelengths. The intensity of the SZ effect is

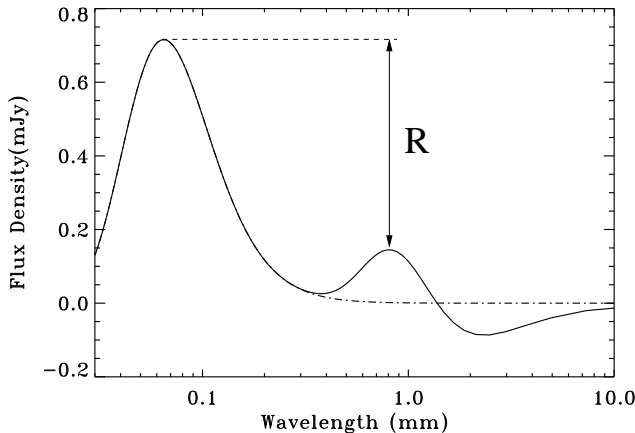


Figure 10. The dash-dotted line shows the spectrum of a grey body ($\beta = 2$) at 50K. The grey body emission has been matched to 5 times the maximum of the SZ emission. The solid line shows the SZ effect with $y = 10^{-4}$ added over the grey dust. We assumed a beam of $5''$. \mathbf{R} is the ratio between the maximum of the dust emission and the maximum of the SZ effect as defined in the text.

fixed by adopting a y parameter of 10^{-4} . The dust emission is given by a grey body with temperature of 50 K and an emissivity of $\beta=1.5$. The amplitude of the dust emission is calculated by varying \mathbf{R} ($\mathbf{R}=0.1,1,5,10,20$). The error bars were estimated by fixing the values of \mathbf{R} and redshift but allowing the temperature to vary between 35 and 65K and the emissivity parameter between 1 and 2.

Figure 11 allows us to examine the behaviour of the mm colours for different redshift ranges:

- Low redshift galaxies ($z \lesssim 1$). In this case the peak of the grey body is far away from the mm range where the signal due to the SZ is dominant (between 1 mm and 3 mm). For $\mathbf{R}=0.1$ we obtain almost the (negative) pure SZ colour $(I(2 \text{ mm})/I(1 \text{ mm})=-0.72, I(3 \text{ mm})/I(1 \text{ mm})=-0.68)$. For higher values of \mathbf{R} the Rayleigh-Jeans tail of the grey body radiation starts to contaminate the SZ spectra producing a shift towards the right top of the $I(2 \text{ mm})/I(1 \text{ mm})$ vs. $I(3 \text{ mm})/I(1 \text{ mm})$ plane, but, for these redshifts, the displacement is modest.
- Intermediate redshift galaxies ($2 \lesssim z \lesssim 5$). This case is similar to the previous one but the grey emission on top of the SZ is more important, producing a larger displacement of the points to the right top corner of the diagram, while the mm colours remain negative.
- High redshift galaxies ($z > 5$). In this case the R-J part of the grey body emission has covered the SZ effect emission at 2 mm, producing in some cases positive $I(2 \text{ mm})/I(1 \text{ mm})$ and $I(3 \text{ mm})/I(1 \text{ mm})$ ratios.

Figure 11 indicates that all points in the bottom left part of the diagram have a dominant SZ component. This diagnostic seems valid up to redshift of several. The accuracy or reliability of the diagnostic will clearly depend on the size of the error bars that in turn depend on the amplitude of the signal and sensitivity of the telescope. All in all it seems that the new facilities would permit to start the exploration of at least the largest star-forming systems at $z < 12$ even if they show moderate dust emission. Inside the estimated error bars, sources dominated by the SZ effect fall clearly

in the distinct quarter of the diagramme where both the 2 to 1 and 3 to 1 mm intensity ratios are negative. This result is very robust in the sense that sources dominated by the SZ are going to be separated from the dust emission independently of redshift. The confusion is higher for high redshift galaxies with the dust emission comparable to the SZ emission.

The diagnostic diagram presented in Figure 11 would be partially covered by future deep surveys at mm wavelengths, showing high redshift sources dominated either by dust or by SZ emission. Because of the expected delay between the burst event and the production of metals and dust, our diagnostic diagramme can potentially be used to constrain the sources and time scales for dust and metal production in the early universe (Morgan & Edmunds 2003).

To further advance in the study of the evolution of the SZ and dust emission in a self-consistent manner, to check in more detail the possibility of observing the SZ through individual galaxies with the next generation of mm telescopes and to estimate the contribution of SZ sources to the background radiation, we will present in a forthcoming paper a set of simulated mm maps including sources dominated by SZ and those dominated by dust emission (with different clustering properties) plus the comparison of our predictions on the SZ background with those made by Aghanim, Balland & Silk (2000) based on the SZ due to black holes-seeded proto-galaxies.

6 CONCLUSIONS

In this paper we have explored the possibility that the central comptonization y parameter in young spheroidal galaxies or galaxies undergoing a massive starforming event may reach values comparable to those observed in galaxy clusters.

However due to the poor angular resolution-sensitivity combination of present day mm facilities, the detection of the SZ effect in individual galaxies may only be possible with the next generation of high angular resolution - high sensitivity mm telescopes (e.g. GTM/LMT or ALMA) and then probably only in the most massive systems capable of producing a $800 \mu\text{m}$ flux of more than a few μJy for periods of time of several hundred megayears.

We have included instrumental noise in our calculations, but neglected the noise contribution caused by high redshift millimeter background point sources (e.g. Blain 1998, Hughes et al. 1998). The confusion due to unresolved sources depends on the actual details (i.e. resolution) of the observation, the (unknown) emission radial profile of these sources and the extrapolation of the number counts to fainter fluxes. Blain et al. (2000) give an estimation of the confusion limit of about $10 \mu\text{Jy}$ for the case of observations at 1 mm and a beam size of $5''$. This value is comparable to the expected SZ flux of galaxies with baryonic masses of $2 \times 10^{12} \text{ M}_\odot$ and an age of $\sim 3 \times 10^8$ years (Figure 7). Confusion will be a major problem when combining independent observations at different frequencies but its effect will be greatly reduced using instruments that simultaneously observe at three selected frequencies.

A major difficulty in the detection of the SZ effect in an individual galaxy will be its confusion with the dust emis-

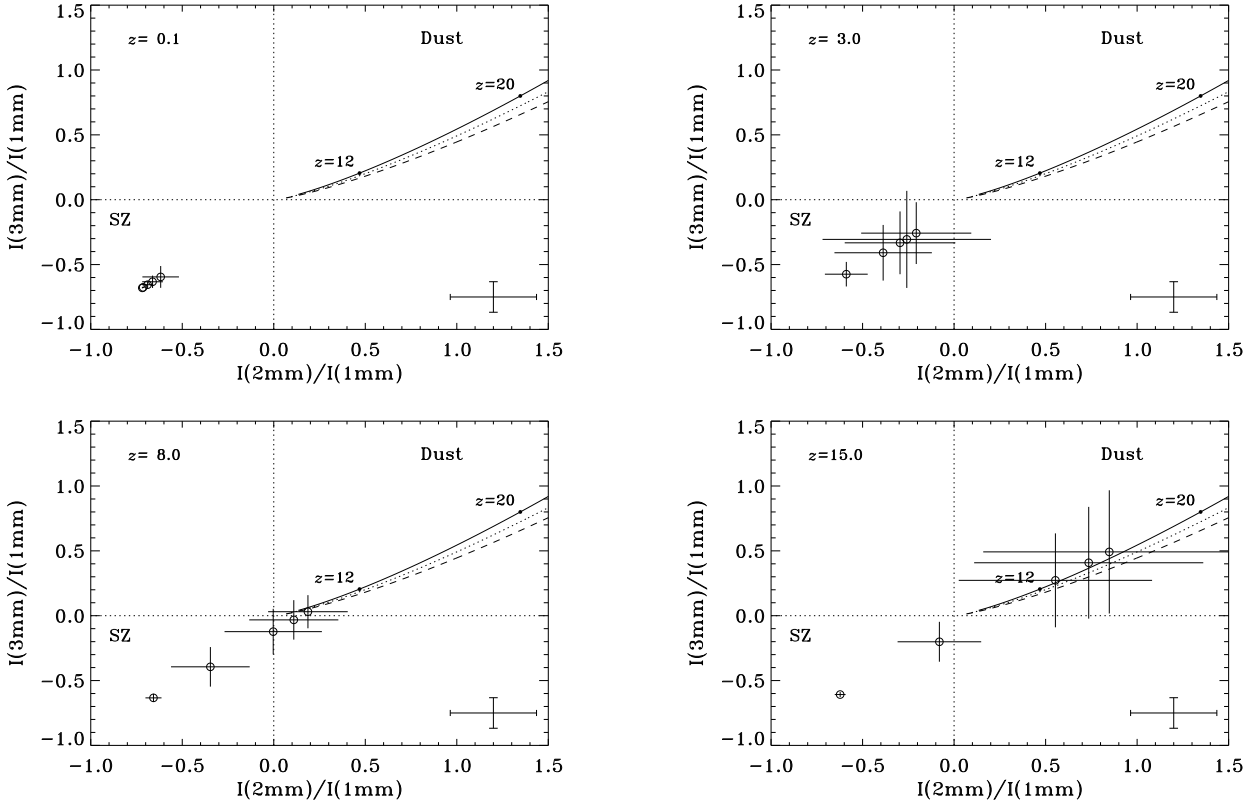


Figure 11. The different panels represent a set of mm colour–colour diagram for sources with both the emission of the SZ effect and the emission from the dust. The different panels correspond to galaxies at different redshifts: $z=0.1$ (top left), $z=3$ (top right), $z=8$ (bottom left) and $z=15$ (bottom right). For each individual panel, the different points correspond to the adopted values of the ratio $R = 0.1, 1, 5, 10, 20$. The amplitude of the bars are calculated by varying the grey body temperature from 35 to 65K and the emissivity parameter from 1 to 2. The lines correspond to $T=50$ K grey body models with emissivity parameters 1 (solid line), 1.5 (dotted line) and 2 (dashed line). The values corresponding to $z=12$ and $z=20$ are indicated. The cross in the bottom right corner corresponds to observational errors for 3σ detection in all three bands.

sion originated in the same star formation event. To solve the dust contamination problem we suggest to exploit the particular spectral signature of the SZ spectrum and maximize its segregation from dust emission by using simultaneous multifrequency observations or differential detection at 1, 2 and 3 mm. In the diagnostic diagram presented in Figure 11 there is a wide region centred at $I(2\text{ mm})/I(1\text{ mm}) = -0.3$ and $I(3\text{ mm})/I(1\text{ mm}) = -0.3$ where the thermal SZ emission can be clearly separated from the dust emission over a wide range of redshifts.

Due to its particular spectrum the detection of the SZ signature in individual galaxies and the discrimination between sources dominated by the SZ effect from those sources dominated by dust emission would be enhanced by the use of differential mapping systems that simultaneously observe at three selected frequencies (Section 3). Additional advantages of such systems will be the lowering of the minimum detected flux due to a better sampling of the time correlated atmospheric fluctuations (i.e. reducing the sky noise) and the relative absence of source confusion generated by dust emitting sources.

New generation of mm cameras such as SCUBA-2 [†]

[†] http://www.roe.ac.uk/atc/projects/scuba_two

or SPEED [‡] – which will have the capability of observing simultaneously in more than a band – would be ideal to detect compact and faint SZ sources.

7 ACKNOWLEDGMENTS

Daniel Rosa González gratefully acknowledges financial support from CONACYT, the Mexican Research Council, as part of ET research grant # 32186-E. At present DRG is supported by POE, a European Research Training Network. Discussions with David Hughes, Richard Ellis, Manolis Pionis and Guillermo Tenorio-Tagle together with useful suggestions from an anonymous referee greatly improved this work.

REFERENCES

Aghanim, N., Blandford, C. and Silk, J. , 2000, *A&A*, 357, 1
 Archibald E. N., Jimenez R., Dunlop J.S., Friaça, A. C. S., McLure R.J., Hughes D.H., 2002, *MNRAS*, 336, 353

[‡] <http://www.astro.umass.edu/~fcrao/instrumentation>

Benson A.J., Frenk C.S., Baugh C.M., Cole S., Lacey C.G., 2001, MNRAS, 327, 1041

Birkinshaw, M. , 1999, Phys. Rept., 310, 97

Blain, A. W., Ivison, R. J. and Smail, I. , 1998, MNRAS, 296, 29

Blain, A. , 1998, MNRAS, 297, 502

Blain, A. , 1999, Science with the Atacama Large Millimeter Array (ALMA)

Blain, A. W., Smail, I., Ivison, R. J., Kneib, J.-P. and Frayer, D. T. , 2002, Physics Reports, 369, 111

Chini, R. and Kruegel, E. and Kreysa, E. and Gemuend, H. - , 1989, A&A, 216, L5

Chini, R. and Kreysa, E. and Biermann, P. L. , 1989, A&A, 219, 87

Church, S., Jaffe, A. and Knox, L. , 2001, CMB and Inflation: the report from Snowmass 2001

Dicker, S. , 2002, Private communication

Diego, J. M., Martínez-González, E., Sanz, J. L., Benítez, N. and Silk, J. , 2002, MNRAS, 331, 556

Dunne, L., Eales, S., Edmunds, M., Ivison, R., Alexander, P. and Clements, D. L. , 2000, MNRAS, 315, 115

Friaca, A. C. S. and Terlevich, R. J. , 1998, MNRAS, 298, 399

Friaca A.C.S., Terlevich R.J., 1999, MNRAS, 305, 90

Friaca A.C.S., Terlevich R.J., 2001, MNRAS, 325, 335

Glenn, J., Bock, J. J., Chattopadhyay, G., Edgington, S. F., Lange, A. E., Zmuidzinas, J., Mauskopf, P. D., Rownd, B., Yuen, L. and Ade, P. A. , 1998, Proc. SPIE Vol. 3357, p. 326-334, Advanced Technology MMW, Radio, and Terahertz Telescopes, Thomas G. Phillips; Ed., 3357, 326

Grevesse N., Sauval A.J., 1998, Space Science Reviews, 85, 161

Gunn, J. E. and Peterson, B. A. , 1965, ApJ, 142, 1633

Holder, G. P. , 2002, ApJ, 580, 36

Holland, W. S., Greaves, J. S., Zuckerman, B., Webb, R. A. , McCarthy, C., Coulson, I. M., Walther, D. M. , Dent, W. R. F., Gear, W. K. and Robson, I. , 1998, Nature, 392, 788

Holweger H., 2001, in Wimmer-Schweingruber R.F., ed., Solar and Galactic Composition. Springer, Berlin, p.23

Hu, E. M., Cowie, L. L. and McMahon, R. G. , 1998, ApJL, 502, 99

Hughes, D. H. and Robson, E. I. and Dunlop, J. S. and Gear, W. K. , 1993, MNRAS, 263, 607

Hughes, D.H. and Gear, W.K. and Robson, E.I. , 1994, MNRAS, 270, 641

Hughes, D. H. and Dunlop, J. S. and Rawlings, S. , 1997, MNRAS, 289, 766

Hughes, D. H., Serjeant, S., Dunlop, J., Rowan-Robinson, M. , Blain, A., Mann, R. G., Ivison, R., Peacock, J. , Efstathiou, A., Gear, W., Oliver, S., Lawrence, A. , Longair, M., Goldschmidt, P. and Jenness, T. , 1998, Nature, 394, 241

Iwamoto K., Brachwitz F., Nomoto K., Kishimoto N., Umeda H., Hix W.R., Thielemann F.-K., 1999, ApJS, 125, 439

Jimenez, R., Friaca, A. C. S., Dunlop, J. S., Terlevich, R. J., Peacock, J. A. and Nolan, L. A. , 1999, MNRAS, 305, 16

Kompaneets, A. S. , 1957, Zh.E.F.T., 31, 876

Lamarre, J. M., Giard, M., Pointecouteau, E., Bernard, J. P., Serra, G., Pajot, F., Désert, F. X., Ristorcelli, I., Torre, J. P., Church, S., Coron, N., Puget, J. L. and Bock, J. J. , 1998, ApJL, 507, L5

Lanfranchi G.A., Friaca A.C.S., 2003, MNRAS, 343, 481

Lisenfeld, U., Isaak, K. G. and Hills, R. , 2000, MNRAS, 312, 433

Levine, E. S., Schulz, A. E. and White, M. , 2002, ApJ, 577, 569

Majumdar, S. , 2001, ApJL, 555, 7

Majumdar, S., Nath, B. B. and Chiba, M. , 2001, MNRAS, 324, 537

Majumdar, S. and Mohr, J. J. , 2003, ApJ, 585, 603

Mauskopf, P. D., Ade, P. A. R., Allen, S. W., Church, S. E., Edge, A. C., Ganga, K. M., Holzapfel, W. L., Lange, A. E., Rownd, B. K., Philhour, B. J. and Runyan, M. C. , 2000, ApJ, 538, 505

Mauskopf, P. D., Ade, P. A. R., Bock, J. J., Church, S. E., Ganga, K. M., Holzapfel, W. L., Philhour, B. J., Wilbanks, T. M. and Lange, A. E , 2003, in preparation

Morgan, H. L. and Edmunds, M. G. , 2003, MNRAS, 343, 427

Natarajan, P. and Sigurdsson, S. , 1999, MNRAS, 302, 288

Navarro, J. F., Frenk, C. S. and White, S. D. M. , 1995, MNRAS, 275, 56

Rephaeli, Y. , 1995, ARAA, 33, 541

Reese, E. D., Carlstrom, J. E., Joy, M., Mohr, J. J., Grego, L. and Holzapfel, W. L. , 2002, ApJ, 581, 53

Rosa-González, D., 2002, Ph.D. Thesis, INAOE, México.

Rosa-González, D., Terlevich, R.J., Terlevich, E., Friaca, A. and Gaztañaga, E. , 2000, Deep Millimeter Surveys: Implications for Galaxy Formation and Evolution, ed. James Lowenthal and David Hughes.

Rosa-González, D., Terlevich, E., Gaztañaga, E., Terlevich, R.J. and Friaca, A. , 2001, A new era in cosmology, ed. Tom Shanks and Nigel Metcalfe.

Rowan-Robinson, M., Mann, R. G., Oliver, S. J., Efstathiou, A., Eaton, N., Goldschmidt, P., Mobasher, B., Serjeant, S. B. G., Sumner, T. J., Danese, L., Elbaz, D., Franceschini, A., Egami, E., Kontizas, M., Lawrence, A., McMahon, R., Norgaard-Nielsen, H. U., Perez-Fournon, I. and Gonzalez-Serrano, J. I. , 1997, MNRAS, 289, 490

Rybicki, G.B. and Lightman, A.P. , 1980, Radiative Processes in Astrophysics, New York: Wiley

Somerville R.S., Primack J.R., 1999, MNRAS, 310, 1087

Spergel, D. N., Verde, L., Peiris, H. V., Komatsu, E., Nolta, M. R., Bennett, C. L., Halpern, M., Hinshaw, G., Jarosik, N., Kogut, A., Limon, M., Meyer, S. S., Page, L., Tucker, G. S., Weiland, J. L. and Wollack, E. and Wright, E. L. , 2003, ApJS, 148, 175

Stanway, E. R., Bunker, A. J. and McMahon, R. G. , 2003, MNRAS, 342, 439

Sunyaev, R. A. and Zel'dovich, Ya. B. , 1972, Comments Astrophys. and Space Sci., 4, 173

Tegmark, M., Silk, J. and Evrard, A. , 1993, ApJ, 417, 54

Telesco, C. M. , 1988, ARAA, 26, 343

van de Hooch L.B., Groenewegen M.A.T., 1997, A&A, 123, 305

Woosley S.E., Weaver T.A., 1995, ApJS, 101, 181

This paper has been produced using the Royal Astronomical Society/Blackwell Science L^AT_EX style file.